

Generation of Ultra-Wideband Multi-Mode Vortex Waves Based on Monolayer Reflective Metasurface

Xiaohang Dong, Hengyi Sun, Changqing Gu*, Zhuo Li, Xinlei Chen, and Baijie Xu

Abstract—In this paper, a monolayer metasurface that can simultaneously generate multi-mode vortex waves in ultra-wideband is proposed. Smooth phase variation is obtained by properly assigning the arm lengths of arrow-shaped metal on the top of the reflective metasurface unit cell. Different reflective cells are arranged in different sectors to form a phase-shifted surface that can convert a linearly polarized plane wave into a vortex wave. The full-wave simulations show that the designed reflective metasurface can generate vortex wave with multi-mode in ultra-wideband from 18 GHz to 42 GHz, which is in good agreement with the theoretical analysis. The proposed reflective metasurface paves an effective approach to generate vortex wave with multi-mode in ultra-wideband for OAM-based systems. Compared to the traditional ways of generating vortex waves, our design has the advantage of wide bandwidth.

1. INTRODUCTION

Vortex electromagnetic wave has helical wavefront. It carries the orbital angular momentum (OAM) and can be expressed by adding the phase factor $e^{-jl\varphi}$ to the plane wave [1]. The topological modes of OAM are mutually orthogonal, which provides theoretically unlimited states for OAM. It paves a new way to solve the problems in the field of communication and imaging [2, 3].

In 1992 Allen et al. found that the Laguerre-Gaussian (LG) modes carry orbital angular momentum [4]. Since then, the OAM has been intensively applied in the domain of optics [5–9]. Recently, OAM has been widely applied in optics, while the researches of OAM in radio frequencies move slowly for a long time. Until 2007, Thidé et al. first numerically showed that vector antenna arrays can produce a vortex wave in a low frequency regime [10]. Then, Mohammadi et al. comprehensively studied the vortex waves generated by a circular antenna array [11]. After that, the researches of OAM in radio frequencies attracted more and more attention. In 2012, Tamburini et al. confirmed that wireless communication via vortex waves could become a reality by experiment [12]. One of the most important aspects of OAM-based communication system is how to generate vortex wave efficiently. There are several approaches to generating vortex wave, such as spiral phase plate [11], antenna arrays [13–15], holographic diffraction gratings [16], circular traveling-wave antenna [17, 18], circular polarized patch [19], dielectric resonate antenna [20], multi-arm spiral patch [21], and metasurfaces [22–29]. Among them, metasurface is extraordinarily promising because of its unprecedented capability of modulating wavefronts of the electromagnetic wave. Metasurface was first used to generate optical vortices based on the generalized laws of reflection and refraction [30]. Although fruitful progress has been achieved toward OAM across both optical and radio frequency domains, vortex wave generations are mostly limited to a narrow frequency band.

For OAM-based systems, it is important to design specific configurations to generate vortex waves. Inspired by the above work, we explore the generation of multimode vortex wave by a metasurface

Received 5 January 2019, Accepted 19 March 2019, Scheduled 9 April 2019

* Corresponding author: Changqing Gu (gucq@nuaa.edu.cn).

The authors are with the Key Laboratory of Radar Imaging and Microwave Photonics, Ministry of Education, College of Electronic and Information Engineering, Nanjing University of Aeronautics and Astronautics, Nanjing 211106, China.

in a wide band. In this paper, we first design a metasurface unit cell that can control the phase of the reflected wave in the range of 0 to 2π . Using this unit cell, we design a metasurface which can produce a single-mode vortex wave in a wide frequency band. Based on the design principle of the single-mode vortex metasurface we give a metasurface model which can generate a multi-mode vortex wave in a wide frequency band. Finally, the proposed metasurfaces are illuminated by a normally incident linearly polarized plane wave. The simulation results show good consistency with the analysis and reach the design expectations.

2. GEOMETRIES OF UNIT AND METASURFACE DESIGN

The metasurface was used to be a vortex wave generator because it can manipulate electromagnetic wave flexibly. In our case, we use the monolayer unit cell, which consists of a metal patch, a dielectric substrate, and a bottom metal backplane for the design of metasurface. With reference to Figure 1, a unit cell of the metasurface has an arrow-shaped metal layer patterned on a dielectric substrate with a relative permittivity of $\epsilon_r = 2.65$. By adjusting the geometric size of the unit cell, we optimize the design of each parameter of the metasurface unit cell and obtain the superior performance of ultra-wideband. The period length of the unit cell is $p = 3$ mm, and the substrate thickness is $d = 1.5$ mm. The metal is set as a perfect electric conductor during the simulation, the thickness of the metal set to $t = 0.035$ mm, and the linewidth is $w = 0.2$ mm. The values of other parameters are $l_o = 2.6$ mm, $h = 0.45$ mm, and $g = 0.8$ mm, respectively.

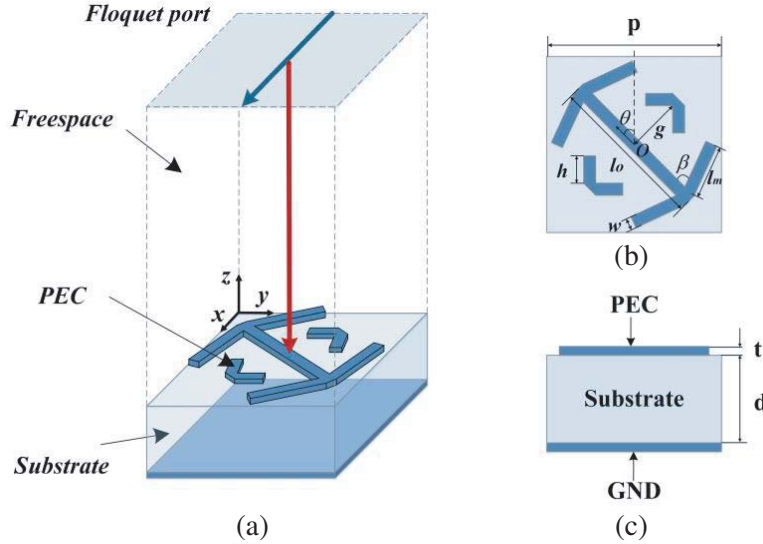


Figure 1. (a) Scheme of the unit used in the design. (b) and (c) are top view and front view of the unit respectively.

With the control of arm length of arrow-shaped metal l_m on the top and rotation angle θ , the unit cell has a reflection phase ranges from 0 to 2π . If we consider twelve units to cover the phase ranges from 0 to 2π . As shown in Figure 2, the phase difference of adjacent elements remains unchanged in the design frequency band, which confirms a good reflection phase response of the unit cell over the frequency range from 18 GHz to 42 GHz. When the rotation angle θ is invariant the reflection phase changes linearly with the arm length, and when the arm length l_m is invariant the phase difference between the two rotating unit cells is π (see Figure 3). By arranging the unit cells with different arm lengths and rotation angles reasonably, we can obtain arbitrary required phase distribution. Actually, the wideband property of the designed metasurface results from a wideband property of the unit cell. The unit cell with an arrow-shaped metal layer patterned on the top can realize multiple resonances at different frequencies, leading to broadband performance.

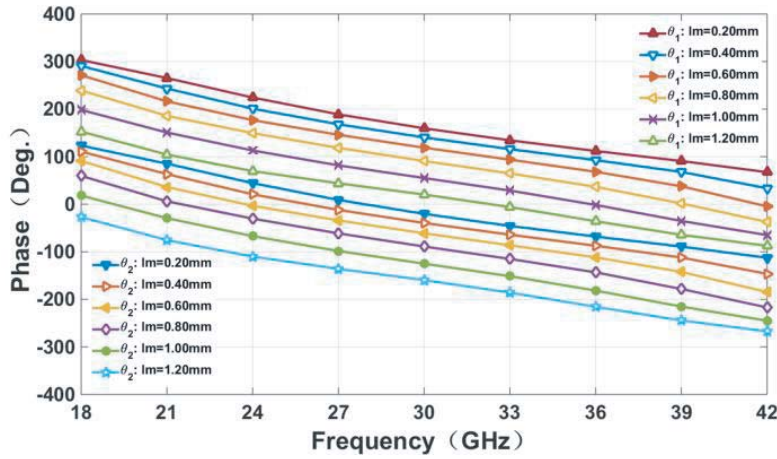


Figure 2. The phase of the reflection coefficient versus the length of the arrow-shaped metal from 18 GHz to 42 GHz. θ_1 means $\theta = \pi/4$, while θ_2 means $\theta = -\pi/4$.

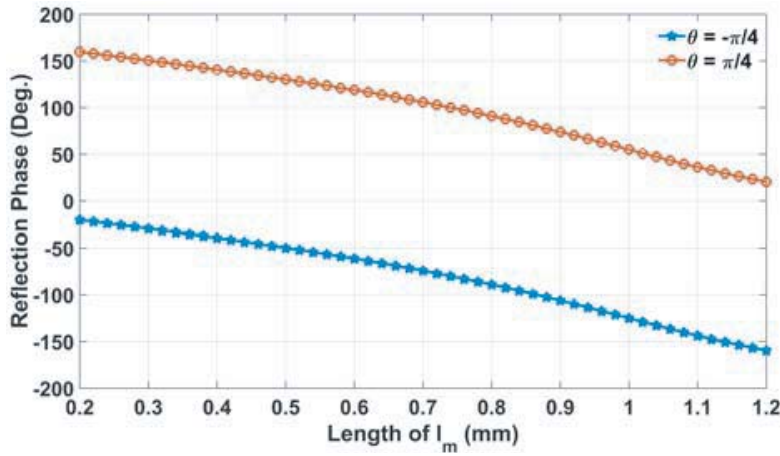


Figure 3. The reflection phase of the cells in two rotation angles ($\theta = \pm\pi/4$) with respect to the arm lengths of arrow-shaped metal l_m .

2.1. Single-Mode Vortex Wave Generation

The generation mechanism of vortex wave is to add a rotating phase factor $e^{-jl\varphi}$ related to the azimuth to the normal electromagnetic wave. For the vortex wave with mode l , when the azimuth angle changes 2π , the phase of the wavefront changes $2\pi l$. We simply arrange N elements around the circle. Each metasurface is composed of multiple concentric rings. The multi-ring structure can be used to make the vortex distribution of the reflected phase map clearer. Then, the phase shift required at each element for the OAM vortex wave at the position $P(x_n, y_n)$ can be obtained by:

$$\phi_n^C(x_n, y_n) = \pm k_0 |\mathbf{r}_f - \mathbf{r}_n| + k_0 \mathbf{r}_n \cdot \hat{\mathbf{u}}_0 \pm l\varphi_n \tag{1}$$

where k_0 is the wave vector, n the position of the unit, r_n the position vector of the element, φ_n the azimuthal angle of the n element on the metasurface.

The linearly polarized plane wave is considered as excitation sources. Therefore, for the position $P(x_n, y_n)$ the compensation phase calculated from Equation (1) is $\phi_n^C(x_n, y_n) = l \cdot \arctan(y_n/x_n)$. After the phase parameter is determined, it is easy to get the layouts of metasurfaces that can generate vortex wave with modes $l = 1$, $l = 2$, and $l = 3$ (see Figure 4) by conducting a geometrical mapping process.

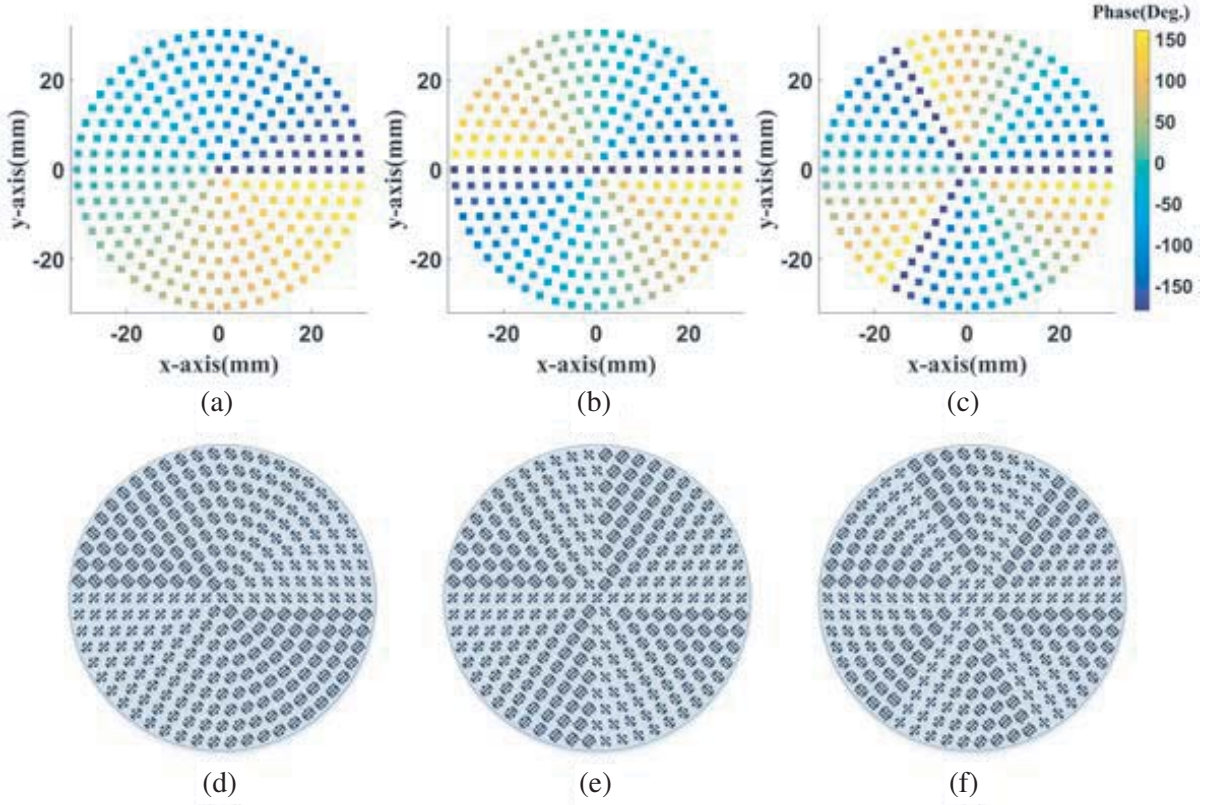


Figure 4. Phase distribution on the metasurface required for generated vortex wave with mode (a) $l = 1$, (b) $l = 2$, and (c) $l = 3$. Scheme of metasurfaces that create a vortex wave with mode (d) $l = 1$, (e) $l = 2$, and (f) $l = 3$. The radius of the substrate is 32.30 mm. Each pattern consists of 10 rings. The metasurface is arranged so as to generate a phase shift that varies azimuthally from 0 to $2\pi l$, thus producing a helicoidal reflected wavefront.

2.2. Multi-Mode Vortex Wave Generation

At present, OAM multiplexing technology is usually considered to improve the capacity and efficiency of communication systems. So, it is necessary to produce multi-mode vortex waves. The vortex wave generated by the traditional OAM antenna is usually a single-mode, and more modes can be obtained only by increasing the number of antennas. With antenna array, the design of the system is difficult, and the cost is expensive. In the case of limited space and cost, the method cannot meet the actual needs. In order to solve the problem, we propose a single metasurface to generate multi-mode vortex wave simultaneously.

The metasurface that can generate a multi-mode vortex wave is proposed in this section, which is assigned with two regions to generate specific modes. As demonstrated numerically, the reflection phases can be controlled by unit cells. When being excited by a plane wave, the reflect-array could be with different values of mode in each region for the generation of $l = 1$ and $l = 3$ modes of vortex wave.

Based on the design principle of the single-mode vortex metasurface, the metasurface unit cells are arranged separately in two different regions. In our case, we consider the 5 inner rings to generate vortex wave with $l = 1$ and the 5 outer rings to generate vortex wave with $l = 3$. As shown in Figure 5, the phase changes 2π in the inner region and 6π in the outer region when it rotates in a circle along the azimuth angle.

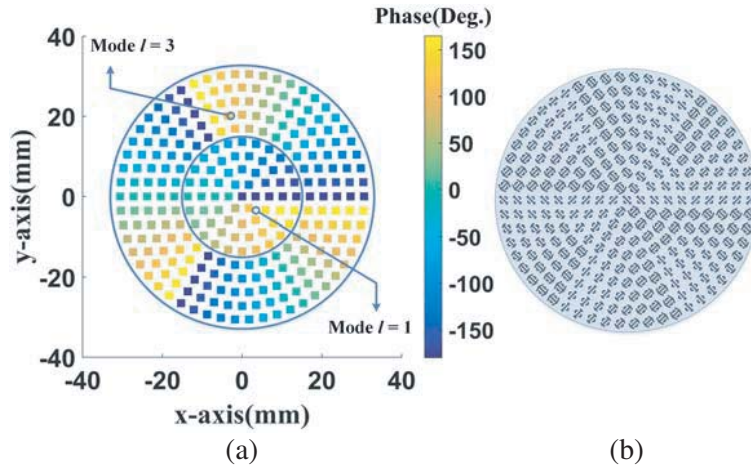


Figure 5. (a) Phase distribution on the metasurface required for generated multi-mode vortex wave. (b) Scheme of metasurface that creates a vortex wave with mode $l = 1$ and $l = 3$ simultaneously. The radius of the substrate is 32.30 mm.

3. SIMULATIONS AND ANALYSIS

Schemes are designed and simulated using CST Microwave Studio. Figure 6 gives the phase distribution and corresponding magnitude distribution of E -field on the observation plane at $z = 250$ mm with different modes at $f = 30$ GHz. Obviously, the vortex wave with an amplitude null exists in the boresight direction in all cases. From these results, we can see that when mode l is larger, the opening

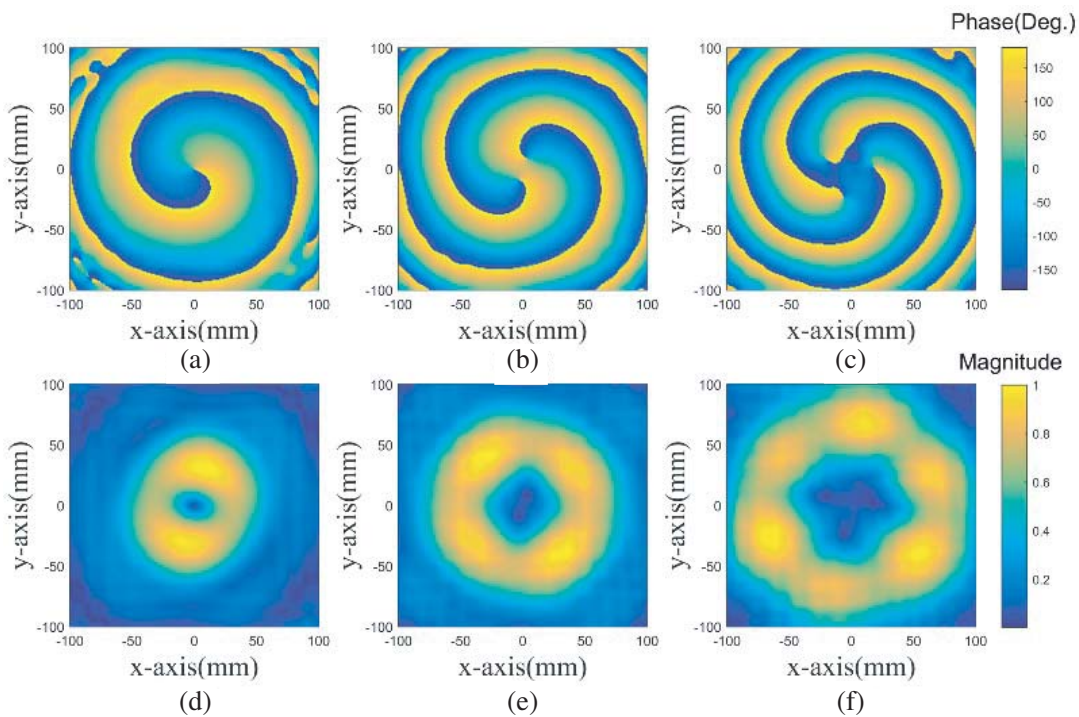


Figure 6. Phase distribution of E -field on the observation plane at $z = 250$ mm with mode (a) $l = 1$, (b) $l = 2$, (c) $l = 3$ and corresponding normalized magnitude distribution with (d) $l = 1$, (e) $l = 2$, and (f) $l = 3$ at $f = 30$ GHz.

angle of the magnitude distribution along the propagation direction gets bigger. By impinging the linearly polarized plane wave on the reflective metasurface array, the wavefront of the reflected wave will be of helical form. Figure 6(a), Figure 6(b), and Figure 6(c) show the phase distributions of a single-arm spiral, a dual-arm spiral, and a three-arm spiral, respectively, which are consistent with the phase characteristics of the vortex wave with mode $l = 1$, $l = 2$, and $l = 3$. The results reveal that vortex wave with different modes l is effectively generated by the proposed metasurface.

To observe bandwidth properties, we present E -field distributions results of the single-mode vortex metasurface with mode $l = 1$ from 18 GHz to 42 GHz in steps of 12 GHz. The phase distribution at different frequency points has the characteristic of vortex wave with mode $l = 1$. The results in Figure 7 show that the single-mode vortex wave can be generated effectively from 18 GHz to 42 GHz.

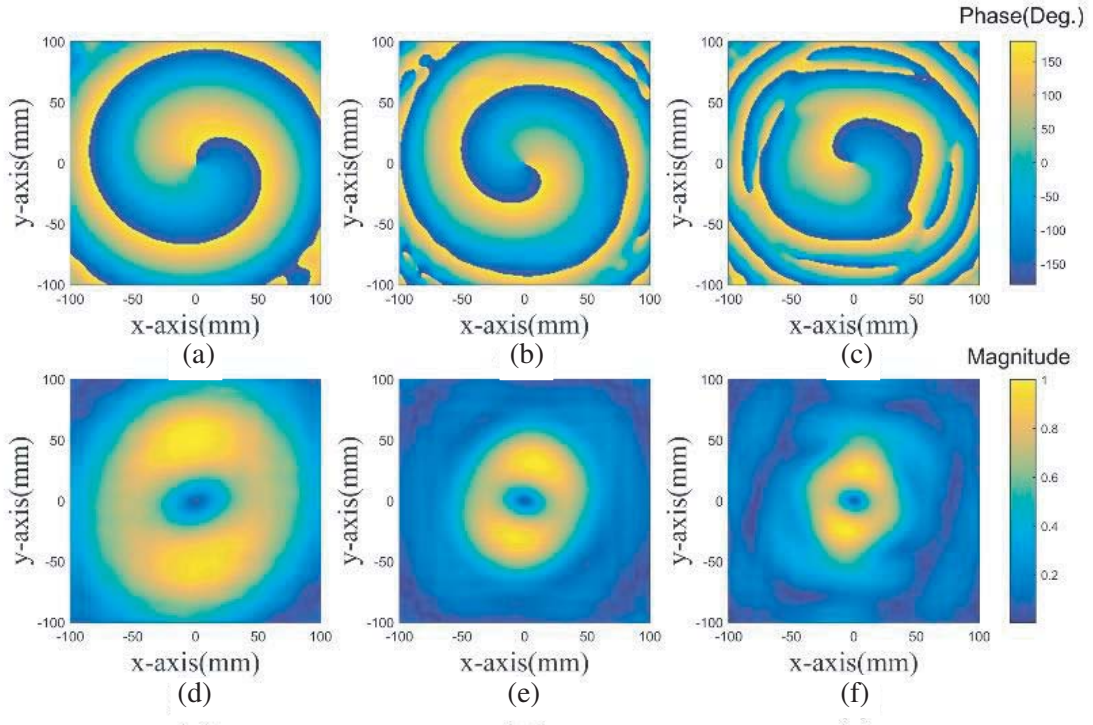


Figure 7. Phase distribution of E -field on the observation plane at $z = 250$ mm with mode $l = 1$ at (a) $f = 18$ GHz, (b) $f = 30$ GHz, (c) $f = 42$ GHz and corresponding normalized magnitude distributions at (d) $f = 18$ GHz, (e) $f = 30$ GHz, (f) $f = 42$ GHz.

The E -field magnitude and phase distributions with mode $l = 3$ at propagation distances of $z = 50$ mm, $z = 150$ mm and $z = 200$ mm are shown in Figure 8. Although the energy of each vortex wave would decrease according to propagation distance, the results of different propagation distances show that the generated vortex wave maintains good stability as it propagates.

The simulation results of single-mode vortex metasurface show that the proposed design method can effectively generate arbitrary mode vortex waves in a wideband, which lays a foundation for the further study of multi-mode vortex metasurface. Then, we consider a multi-mode metasurface illuminated by a linearly polarized incident wave. The simulated E -field results are shown in Figures 9–11, which verify the good performance of the proposed designs.

Take the results at $f = 18$ GHz as an example. Figure 9(a) is the phase distribution in near fields of the multi-mode metasurface. In theory, the simulation results only contain modes $l = 1$ and $l = 3$, i.e., the results of multi-mode and cumulative results of single-mode should be consistent. Consider filtering out mode $l = 3$ from multi-mode results. As illustrated in Figure 9(b), the remaining phase distribution is the same as that of mode $l = 1$. The phase distribution after filtering out mode $l = 1$ from multi-mode results is presented in Figure 9(c). The phase distribution in mode $l = 3$ can be recognized clearly. The

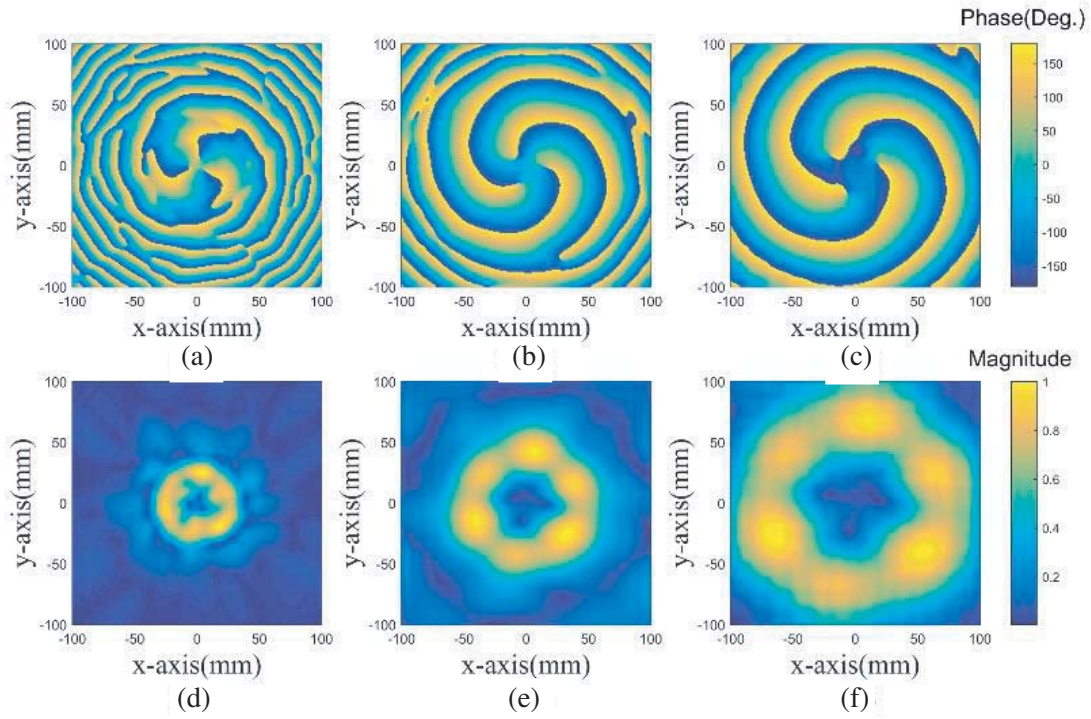


Figure 8. Phase and corresponding normalized magnitude distributions of E -field on the observation plane at (a), (d) $z = 50$ mm, (b), (e) $z = 150$ mm and (c), (f) $z = 250$ mm with mode $l = 3$ at $f = 30$ GHz.

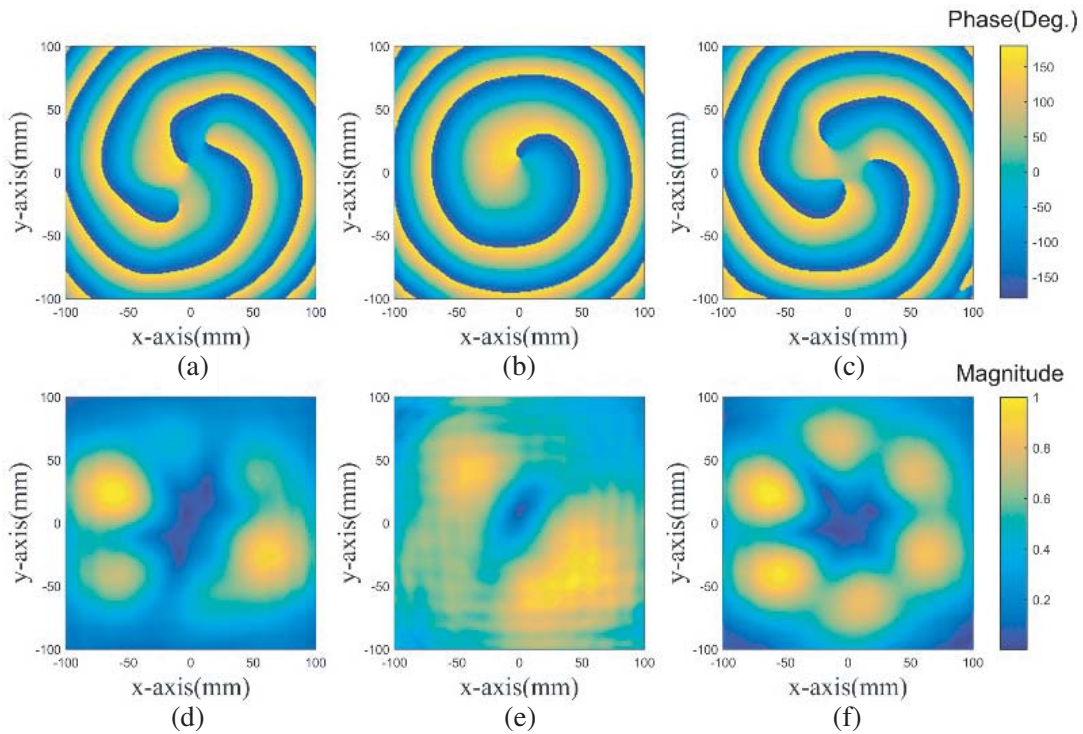


Figure 9. (a) Phase distribution of E -field on the observation plane at $z = 150$ mm with mode $l = 1$ and $l = 3$ at $f = 18$ GHz. (b) multi-mode result reducing single-mode $l = 3$ result. (c) multi-mode result reducing single-mode $l = 1$ result and (d), (e), (f) corresponding normalized magnitude distribution.

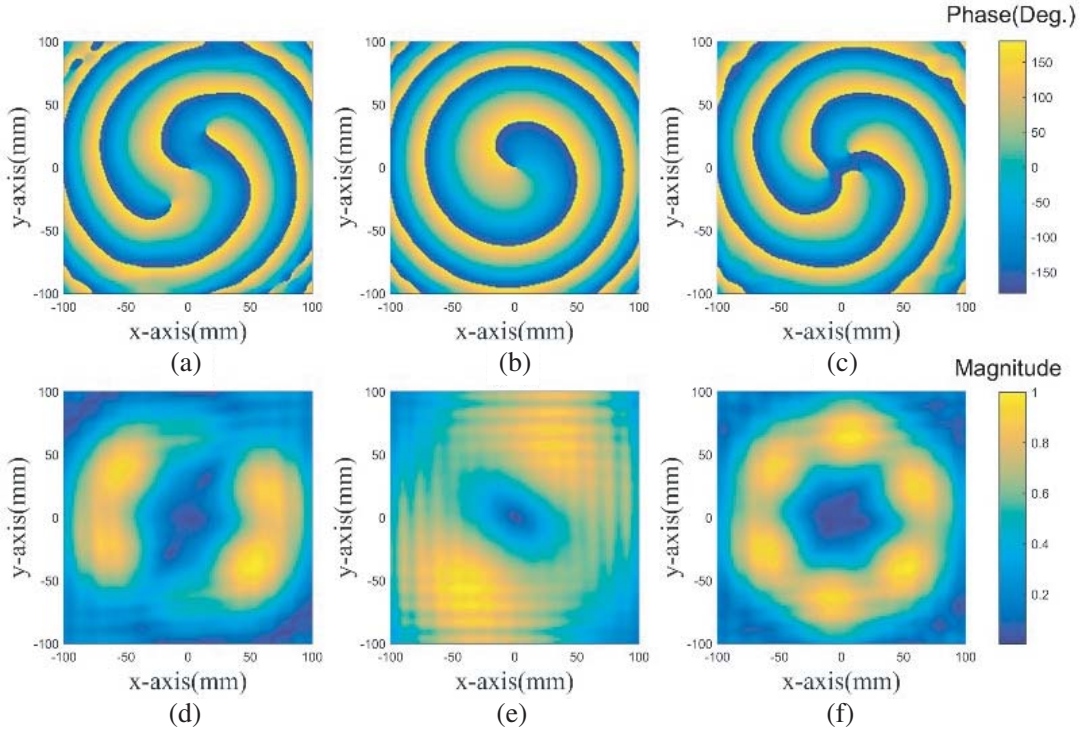


Figure 10. (a) Phase distribution of E -field on the observation plane at $z = 250$ mm with mode $l = 1$ and $l = 3$ at $f = 30$ GHz. (b) multi-mode result reducing single-mode $l = 3$ result. (c) multi-mode result reducing single-mode $l = 1$ result and (d), (e), (f) corresponding normalized magnitude distribution.

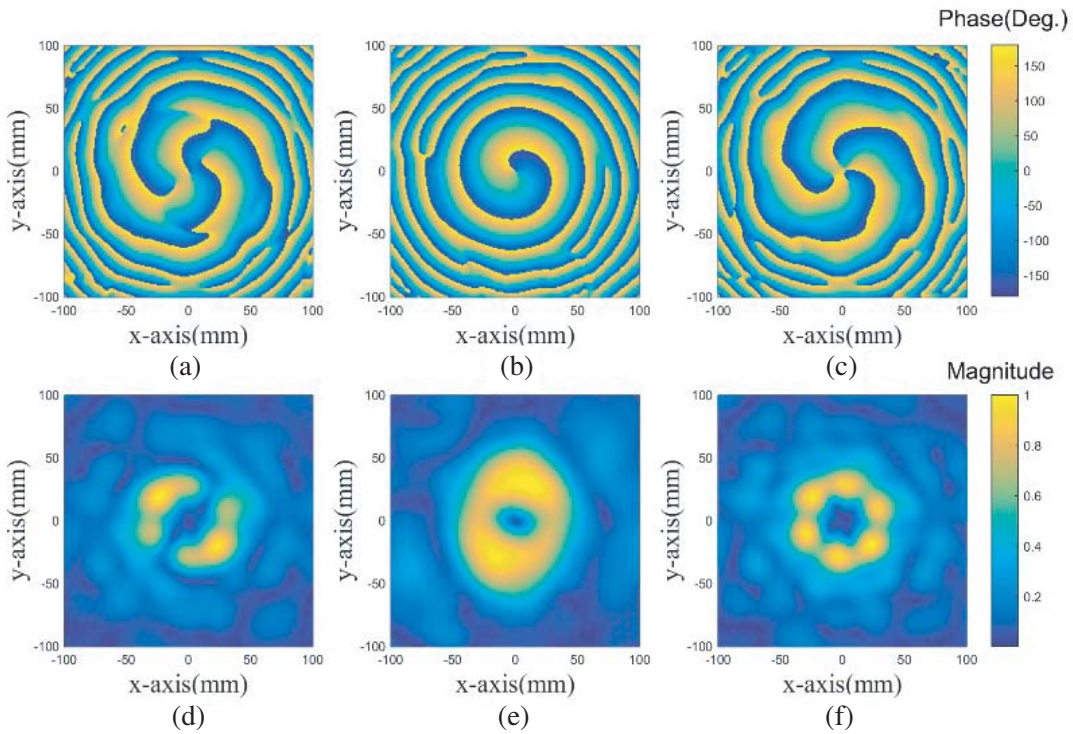


Figure 11. (a) Phase distribution of E -field on the observation plane at $z = 250$ mm with mode $l = 1$ and $l = 3$ at $f = 42$ GHz. (b) multi-mode result reducing single-mode $l = 3$ result. (c) multi-mode result reducing single-mode $l = 1$ result and (d), (e), (f) corresponding normalized magnitude distribution.

results at $f = 30$ GHz and $f = 42$ GHz are consistent with the foregoing at $f = 18$ GHz. Figures 9–11 reveal that the designed ring coaxial metasurface can produce vortex waves of multi-modes at the same time.

4. CONCLUSION

In conclusion, by arranging the metasurface unit cells in concentric circles, we propose a simple design to generate vortex wave based on metasurface in ultra-wideband from 18 GHz to 42 GHz. The proposed design is verified by simulation, and the simulation results agree well with the theoretical predictions. It is found that single-mode $l = 1$, $l = 2$, $l = 3$ and multi-mode vortex wave can be generated when the proposed metasurfaces are illuminated by a linearly polarized plane wave. The proposed metasurface reflectarray is promising for future applications in OAM-based communication systems. Compared with previous work, which can only produce one mode at a certain frequency point or in a very narrow frequency band, the proposed vortex metasurfaces possess more modes and work in a wider band. This work is not only an expansion to the applications of metasurface, but also a simplifier of the vortex wave generation.

ACKNOWLEDGMENT

The authors thank the support from the Foundation of Graduate Innovation Center in NUAU under Grant No. kfjj20170414, the Fundamental Research Funds for the Central Universities, National Natural Science Foundation of China (61501227, 61071019), Postdoctoral Science Foundation of China (2015M581789), 56YAH17032 of NUAU, Jiangsu Innovation Program for Graduate Education (KYLX16-0370), Fundamental Research Funds for the Central Universities (NJ20160011), MINECO-Spain (TEC2016-75650-R), Generalitat de Catalunya (2017SGR-1159) and FEDER funds. The authors also acknowledge the China Scholarship Council (CSC) for Grant 201706830064.

REFERENCES

1. Beth, R. A., "Mechanical detection and measurement of the angular momentum of light," *Physical Review*, Vol. 50, No. 2, 115–125, 1936.
2. Wang, J., J. Y. Yang, I. M. Fazal, N. Ahmed, Y. Yan, H. Huang, et al., "Terabit free-space data transmission employing orbital angular momentum multiplexing," *Nature Photonics*, Vol. 6, No. 7, 488–496, 2012.
3. Liu, K., Y. Cheng, Y. Gao, X. Li, Y. Qin, and H. Wang, "Super-resolution radar imaging based on experimental OAM beams," *Applied Physics Letters*, Vol. 110, No. 16, 164102, 2017.
4. Allen, L., M. W. Beijersbergen, R. J. Spreeuw, and J. P. Woerdman, "Orbital angular momentum of light and the transformation of Laguerre-Gaussian laser modes," *Physical Review & Atomic Molecular & Optical Physics*, Vol. 45, No. 11, 81–85, 1992.
5. Gibson, G., et al., "Free-space information transfer using light beams carrying orbital angular momentum," *Optics Express*, Vol. 12, No. 22, 5448–5456, 2004.
6. Grier, G. and M. D. Grier, "A revolution in optical manipulation," *Nature*, Vol. 424, No. 6950, 810–816, 2003.
7. Anzolin, G., F. Tamburini, A. Bianchini, G. Umbriaco, and C. Barbieri, "Optical vortices with starlight," *Astronomy & Astrophysics*, Vol. 488, No. 3, 1159–1165, 2008.
8. Berkhout, G. C. G. and M. W. Beijersbergen, "Method for probing the orbital angular momentum of optical vortices in electromagnetic waves from astronomical objects," *Physical Review Letters*, Vol. 101, No. 10, 100801, 2008.
9. Guan, B., C. Qin, R. P. Scott, N. K. Fontaine, T. Su, R. Proietti, et al., "Polarization diversified integrated circuits for orbital angular momentum multiplexing," *IEEE Photonics Technology Letters*, Vol. 27, No. 10, 1056–1059, 2015.
10. Thidé, B., et al., "Utilization of photon orbital angular momentum in the low-frequency radio domain," *Physical Review Letters*, Vol. 99, No. 8, 087701, 2007.

11. Mohammadi, S. M., et al., "Orbital angular momentum in radio — A system study," *IEEE Transactions on Antennas & Propagation*, Vol. 58, No. 2, 565–572, 2010.
12. Tamburini, F., et al., "Experimental demonstration of free-space information transfer using phase modulated orbital angular momentum radio," *Physics*, Vol. 13, No. 2, 20–25, 2013.
13. Brousseau, C., K. Mahdjoubi, O. Emile, and W. Wei, "Generation of OAM waves with circular phase shifter and array of patch antennas," *Electronics Letters*, Vol. 51, No. 6, 442–443, 2015.
14. Gaffoglio, R., A. Cagliero, A. D. Vita, and B. Sacco, "OAM multiple transmission using uniform circular arrays: Numerical modeling and experimental verification with two digital television signals," *Radio Science*, Vol. 51, No. 6, 645–658, 2016.
15. Bai, Q., A. Tennant, B. Allen, and M. U. Rehman, "Generation of Orbital Angular Momentum (OAM) radio beams with phased patch array," *Antennas & Propagation Conference*, Vol. 9, No. 6, 410–413, 2014.
16. Tamburini, F., et al., "Encoding many channels in the same frequency through radio vorticity: First experimental test," *New Journal of Physics*, Vol. 14, No. 3, 811–815, 2011.
17. Zhang, Z., S. Zheng, X. Jin, H. Chi, and X. Zhang, "Generation of plane spiral OAM waves using traveling-wave circular slot antenna," *IEEE Antennas & Wireless Propagation Letters*, Vol. 16, 8–11, 2016.
18. Zhang, W., S. Zheng, X. Hui, Y. Chen, X. Jin, H. Chi, et al., "Four-OAM-mode antenna with traveling-wave ring-slot structure," *IEEE Antennas & Wireless Propagation Letters*, Vol. 16, 521–524, 2017.
19. Barbuto, M., F. Trotta, F. Bilotti, and A. Toscano, "Circular polarized patch antenna generating orbital angular momentum," *Progress In Electromagnetics Research*, Vol. 148, 23–30, 2014.
20. Liang, J. and S. Zhang, "Orbital Angular Momentum (OAM) generation by cylinder dielectric resonator antenna for future wireless communications," *IEEE Access*, Vol. 4, 9570–9574, 2016.
21. Mao, F., M. Huang, T. Li, J. Zhang, and C. Yang, "Broadband generation of orbital angular momentum carrying beams in RF regimes," *Progress In Electromagnetics Research*, Vol. 160, 19–27, 2017.
22. Yu, S., L. Li, G. Shi, C. Zhu, X. Zhou, and Y. Shi, "Design, fabrication, and measurement of reflective metasurface for orbital angular momentum vortex wave in radio frequency domain," *Applied Physics Letters*, Vol. 108, No. 12, 5448, 2016.
23. Yu, S., G. Shi, C. Zhu, and Y. Shi, "Generating multiple orbital angular momentum vortex waves using a metasurface in radio frequency domain," *Appl. Phys. Lett.*, Vol. 108, No. 24, 241901, 2016.
24. Jin, J., et al., "Generation and detection of orbital angular momentum via metasurface," *Scientific Reports*, Vol. 6, 24286, 2016.
25. Chen, M. L. N., L. J. Jiang, and W. E. I. Sha, "Artificial perfect electric conductor-perfect magnetic conductor anisotropic metasurface for generating orbital angular momentum of microwave with nearly perfect conversion efficiency," *Journal of Applied Physics*, Vol. 119, No. 6, 064506, 2016.
26. Chen, M. L. N., L. J. Jiang, and W. E. I. Sha, "Ultrathin complementary metasurface for orbital angular momentum generation at microwave frequencies," *IEEE Transactions on Antennas & Propagation*, Vol. 65, No. 1, 396–400, 2017.
27. Chen, M., L. J. Jiang, and W. E. I. Sha, "Detection of orbital angular momentum with metasurface at microwave band," *IEEE Antennas & Wireless Propagation Letters*, Vol. 17, No. 1, 110–113, 2018.
28. Xu, H. X., H. Liu, X. Ling, Y. Sun, and F. Yuan, "Broadband vortex wave generation using multimode pancharatnam-berry metasurface," *IEEE Transactions on Antennas & Propagation*, Vol. 65, No. 12, 7378–7382, 2017.
29. Zhang, Y., L. Yang, H. Wang, X. Zhang, and X. Jin, "Transforming surface wave to propagating OAM vortex wave via flat dispersive metasurface in radio frequency," *IEEE Antennas & Wireless Propagation Letters*, Vol. 17, No. 1, 172–175, 2018.
30. Yu, N., et al., "Light propagation with phase discontinuities reflection and refraction," *Science*, Vol. 334, 333–337, 2011.